A Local Constraint Method for Needle Insertion Modeling and Simulation

Lijuan Wang, Shinichi Hirai
Department of Robotics
Ritsumeikan University
Noji-higashi 1-1-1 Kusatsu Shiga, Japan
Emails: gr0081vf@ed.ritsumei.ac.jp
hirai@se.ritsumei.ac.jp

Abstract—**This paper presents a novel constraint method for dynamic modeling and simulation of needle insertion based on FE framework. Modeling of the interactive events during a needle insertion procedure such as contact, puncture and friction using the finite element method is cumbersome due to the need to continually update the mesh to match the geometry of the discontinuity. Here, we describe a Local Constraint Method that uses outputs generated by the interaction between a needle node and a 'contact' point inside one finite element of the tissue as constraints that affect deformation and the force distribution of the tissue and needle. The constraints are applied at the nodal points of the initial mesh in order to avoid remeshing; and the variations mapped from the needle to points within the tissue region are considered as properties representative of the whole body to ensure accuracy of the simulation. This method can be employed to simulate a dynamic model for different interactions with different material properties. A simulation based on this method to realize the dynamic model of needle insertion is described for validation.**

Keywords-needle insertion; FEM; dynamic model; soft tissue; simulation

I. INTRODUCTION

Modern clinical practice in procedures such as biopsies, prostate brachytherapy and neurosurgery often involves deep insertion of needle-like tools into soft inhomogeneous tissues [1]. Accurate orientation beneath the tissue surface during these procedures is difficult to achieve due to tissue deformation, and unknown interactions between the tools and the tissues. Modeling and simulations representing such interactions between surgical tools and deformable tissues have been developed in recent years, with the aim to understand the forces and geometric changes involved in medical application, such as in robot-assisted surgery, and develop virtual surgical systems for training and planning. Constructing appropriate mechanics-based models to simulate the interactive behaviors of needle and tissues during insertion has been found challenging.

Over the past two decades, experimental and analytical models that characterize tissue properties, needle forces, needle deflection and the mechanics of events during needle insertion, such as contact, rupture and friction, have been improved. DiMaio *et al.* developed a 2D FE model applying force distribution along the needle shaft to measure planar tissue deformation in a soft tissue phantom using a linear elastostatic material model [2]. They used fast low-rank matrix updates to achieve the interaction simulation [3]. Alterovitz *et al.* proposed a dynamic contact model for needle insertion using a spring model and showed that faster needle insertion improves accuracy in positioning a needle [4]. Nienhuys *et al.* improved on a computational method for the simulation using finite element method (FEM) in both 2D and 3D [5]. Okamura *et al.* developed an empirical force model for soft tissue penetration. The needle forces were considered as a combination of stiffness force, friction and cutting forces [6]. Using a load cell developed for their experimental apparatus [7], Kataoka *et al.* showed the combined behavior of needle forces, which included those at the tip and those along the shaft that were independently measured. Webster *et al.* presented a bevel-tip needle steering model [8] and Misra *et al.* described a mechanics-based needle steering model predicting interactions at the needle tip and overall needle bending with consideration to the geometry of the needle tip and the material properties [9]. Mahvash and Dupont *et al.* contributed to knowledge of the mechanics of rupture events with a dynamic model [10]. They showed that a higher velocity of needle insertion reduces the force of a rupture event.

In this paper, to simulate needle-tissue interactions we considered the procedure of needle insertion as a combination of contact, rupture and friction forces respective to the needle tip and shaft. A Local Constraint Method (LCM) was applied to avoid the need to remesh which is normally required due to conflict between the continuous movement of the needle and discontinuous FE frameworks. We present the principles and details of our approach and propose its application for dynamic modeling and simulation of needle insertion.

This paper is arranged as follows. In section 2, the insertion procedure analysis is described. Section 3 details the modeling and simulation method using local constraints. Section 4 shows results of our simulations. Conclusions and future work appear in the final section.

II. INSERTION PROCEDURE ANALYSIS

The procedure of needle insertion into a soft tissue has always been separated into several events including contact, puncture, cutting, and release. However the actual puncture event is more complicated than previously imagined. A typical

978-1-4577-0499-4/11/$26.00 ©2011 IEEE

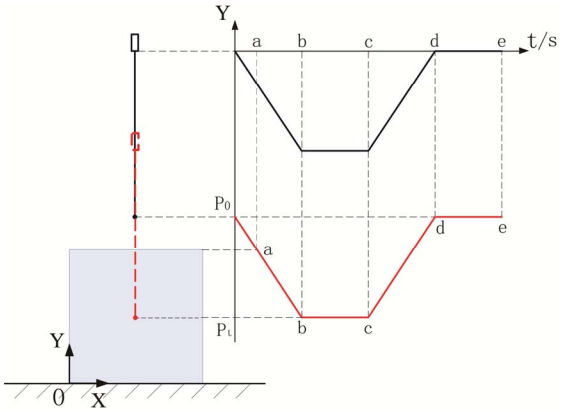

Figure 1. Example of an insertion procedure

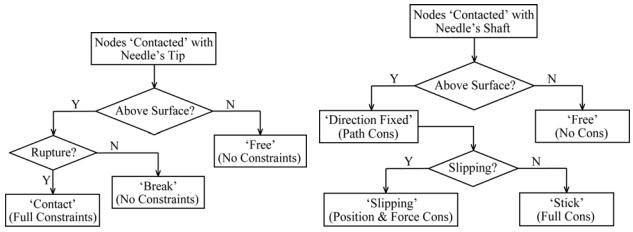

(a) (b)

Figure 2. Insertion procedure for interaction simulation respective to constraints (a) tip node, (b) shaft node.

needle insertion procedure is depicted in Figure 1. As the needle contacts the surface (a), the tissue is deformed with increasing interaction forces between the two objects. When needle-tip forces exceed the tissue puncture threshold, rupture occurs. As the needle enters the tissue, both friction along the needle shaft and the rupture occur independently, according to their respective conditions. Even while the needle is static within the tissue (b-c), rupture and friction events are still present occasionally, and also as it is removed (c-d-e).

To accommodate different functions of needle-tissue interactions and geometric properties, we considered forces on the 'needle' at two different kinds of nodes, the tip node and the shaft nodes. The events of contact, puncture and friction are considered to be related to these different parts of the needle, consequently different constraints are applied to the two kinds of nodes according to boundary conditions of the events, such as the geometric boundary of the surface, the threshold of puncture and the critical relative velocity for friction, Figure 2(a) and 2(b). As a result, dealing with these constraints becomes a major issue to be addressed during simulation. For the sake of simplicity, we describe the insertion progress of a thin and inflexible needle into a uniform isotropic tissue with viscoelastic material behavior.

III. DYNAMIC MODEL FOR NEEDLE-TISSUE INTERACTION

Modeling and simulation of needle-tissue interaction using FEM is challenging because the invasive process involves multiple remeshing which is computationally expensive for

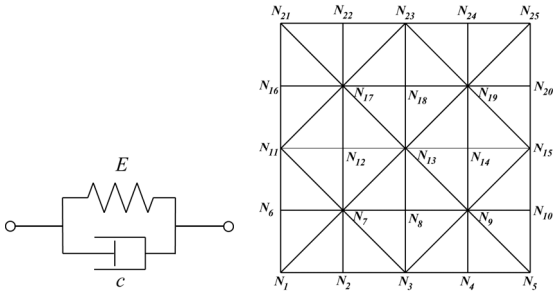

(a) (b)

Figure 3. (a). Kelvin-Voigt Model used to describe the viscoelastic force-deformation behavior in virtual tissue. (b) 2D FE mesh with 25 mass points and 32 triangle elements.

simulation [11]. In this section, we describe a local constraint method that avoids the need to remesh. This method is applied to achieve interactive needle insertion using a 2D viscoelastic tissue model for simulation. A deformable tissue model with viscoelastic behavior is proposed.

A. *Deformable Tissue Model*

The tissue model is represented by a serial connection Kelvin-Voigt Model with viscoelastic behavior, Figure 3(a). The FE mesh used to simulate the deformation consists of 5×5 nodal points and 32 triangles, Figure 3(b). The 'tissue' body is assumed to be uniform and isotropic. Four parameters: the Lamé's constants λ^{ela}, μ^{ela} and λ^{vis}, μ^{vis}, that characterize the elasticity and viscosity respectively for each triangle, are determined by:

$$\lambda^{ela} = \frac{E\upsilon^{ela}}{(1+\upsilon)(1-2\upsilon)},\ \mu^{ela} = \frac{E}{2(1+\upsilon)}$$
$$\lambda^{vis} = \frac{\nu^{vis} c}{(1+\upsilon^{vis})(1-2\upsilon^{vis})},\ \mu^{vis} = \frac{c}{2(1+\upsilon^{vis})}, \quad (1)$$

where E and c are the elastic and viscous moduli and Poisson ratios are given by υ and υ^{vis}.

If u_N denotes the displacement vector of all nodal points, and $\dot{u}_N$ denotes the vector of velocity, J_λ and J_μ as the whole connection matrices which can be obtained by synthesizing partial matrices together to describe the geometric relationship within the total mesh structure, the internal forces can be formulated as:

$$F_{visela} = \left(\lambda^{ela} J_\lambda + \mu^{ela} J_\mu\right) u_N + \left(\lambda^{vis} J_\lambda + \mu^{vis} J_\mu\right) \dot{u}_N . \quad (2)$$

We suppose that one side of the tissue is fixed during the simulation. Applying the constraint stabilization method (CSM) to generate constraints of these fixed nodes [12], we finally have

$$A^T \ddot{u}_N + 2\omega A^T \dot{u}_N + \omega^2 A^T u_N = 0 \quad (3)$$

as constraints on the bottom, where A is the constraint matrix by which we selected the nodes to be fully constrained. The dynamic equations of motion can be written as follows:

$$\begin{cases} M\ddot{u}_N = -F_{visela} + F_{ext} + \lambda A \\ A^T \ddot{u}_N + 2\omega A^T \dot{u}_N + \omega^2 A^T u_N = 0 \end{cases}, \quad (4)$$

where λ is the Lagrange multiplier and M denotes the inertia matrix. The constraint equation here is only for the external constraints of the fixed nodes. To demonstrate effects from the needle, different types of constraints at interactive nodes are added, including the modification of the external force vector F_{ext} and the displacement constraint matrix A according to different situations.

B. Local Constraint Method

When needle-tissue interactions occur, the most important issue is to deal with the constraints (including external forces and displacement constraints) applied to the two objects. We propose the constraint method for interaction simulation to avoid having to continually remesh throughout the needle insertion procedure to improve accuracy.

Our solution is to use a 'local-region', as an intermediate between the needle and the whole tissue body, which is inside one finite element when the needle node is considered to be 'reached' within this region, rather than at the node. Global constraints can be obtained from the 'local-region' instead of the 'point-to-point' influences in order to realize the interactive simulation. The centroid in the local region has been chosen to be the middle point for mapping. The scheme of this method can be separated into two parts, Figure 4. One is to transfer the displacements and forces between the element centroid and the 'needle contact' tissue point which is not present in the FE frame of the tissue. The other is to calculate the reaction forces between vertices of the element $P_i\ P_j\ P_k$ and the centroid P_{cent} as a sub-system caused by instantaneous change at the center considering behavior of the material inside the local region.

For instance, the local constraint mapping process can be considered as 3 steps as follows:

1) Step I: Displacement from Tip to Centroid

The instantaneous displacement of the needle tip u_{tip} is regarded as the input of the local region system, Figure 4 (a). Considering the material behavior inside the triangular element, we assume that at the moment we calculate the constraint the body inside the deformed triangle is uniform and has the same viscoelastic behavior as the whole body. Current coordinates of nodal points $P_i\ P_j\ P_k$ and P_{tip} in deformed shape are defined as (ξ_i^*, η_i^*), (ξ_j^*, η_j^*), (ξ_k^*, η_k^*) and (ξ_{tip}^*, η_{tip}^*). We can linearly approximate the displacement inside the triangle as below:

$$u(\xi,\eta) = u_i N_{i,j,k}(\xi,\eta) + u_j N_{j,k,i}(\xi,\eta) + u_k N_{k,i,j}(\xi,\eta), \quad (5)$$

where the shape function $N_{i,j,k}$, similarly with $N_{j,k,i}$ and $N_{k,i,j}$, is defined as:

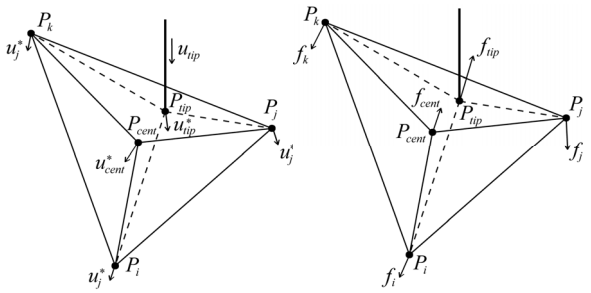

(a) (b)

Figure 4. Scheme of the Local Constraint Method

$$N_{i,j,k}(\xi,\eta) = \frac{\Delta PP_jP_k}{\Delta P_iP_jP_k}, \quad (6)$$

where

$$\Delta P_iP_jP_k = \frac{(\xi_i\eta_j - \eta_i\xi_j) + (\xi_j\eta_k - \eta_j\xi_k) + (\xi_k\eta_i - \eta_k\xi_i)}{2},$$

So we have

$$\begin{aligned} u_{cent}^* &= u_i^* N_{i,j,k}^{cent*} + u_j^* N_{j,k,i}^{cent*} + u_k^* N_{k,i,j}^{cent*} \\ u_{tip}^* &= u_i^* N_{i,j,k}^{tip*} + u_j^* N_{j,k,i}^{tip*} + u_k^* N_{k,i,j}^{tip*}, \end{aligned} \quad (7)$$

where, superscript * denotes instantaneous displacements of points in the triangle, and the shape functions can be calculated as

$$\begin{aligned} N_{i,j,k}^{cent*} &= N_{i,j,k}^*(\xi_{cent}^*, \eta_{cent}^*) = \frac{\Delta P_{cent}^* P_j^* P_k^*}{\Delta P_i^* P_j^* P_k^*}, \\ N_{i,j,k}^{tip*} &= N_{i,j,k}^*(\xi_{tip}^*, \eta_{tip}^*) = \frac{\Delta P_{tip}^* P_j^* P_k^*}{\Delta P_i^* P_j^* P_k^*}. \end{aligned}$$

Note that the shape functions of the centroid equal each other as a constant

$$\begin{aligned} N_{i,j,k}^{cent*} &= N_{j,k,i}^{cent*} = N_{k,i,j}^{cent*} \\ &= \frac{\Delta P_{cent}^* P_j^* P_k^*}{\Delta P_i^* P_j^* P_k^*} = \frac{\Delta P_{cent} P_j P_k}{\Delta P_i P_j P_k} \equiv \frac{1}{3}, \end{aligned}$$

we have $u_{cent}^* = \frac{1}{3}(u_i^* + u_j^* + u_k^*)$, combining with the tip point in (7), which directly yields

$$u^*_{cent} = \left(\frac{1}{3} - N^{tip*}_{i,j,k}\right)u^*_i + \left(\frac{1}{3} - N^{tip*}_{j,k,i}\right)u^*_j + \left(\frac{1}{3} - N^{tip*}_{k,i,j}\right)u^*_k + u^*_{tip}. \quad (8)$$

Similarly the velocity of the centroid point is approximated as:

$$\dot{u}^*_{cent} = \left(\frac{1}{3} - N^{tip*}_{i,j,k}\right)u^*_i + \left(\frac{1}{3} - N^{tip*}_{j,k,i}\right)\dot{u}^*_j + \left(\frac{1}{3} - N^{tip*}_{k,i,j}\right)\dot{u}^*_k + \dot{u}^*_{tip}. \quad (9)$$

2) Step II: $u^*_{cent} \rightarrow F_{i,j,k}$ & f_{cent}

The force-displacement behavior of the viscoelastic tissue has been considered to solve the dynamic equation of motion (4) inside a Local Constraint Region (LCR), Figure 5., which comprises the three apexes and centroid of a triangle. Stiffness and damping matrices of these sub-triangles can be calculated in advance as:

$$K_s = \lambda^{ela} J^{\lambda}_s + \mu^{ela} J^{\mu}_s$$
$$B_s = \lambda^{vis} J^{\lambda}_s + \mu^{vis} J^{\mu}_s, \quad s = 1 \sim 4.$$

Matrices J^{λ}_s and J^{μ}_s are referred to as partial connection matrices of geometrical-based sub-triangles including no physical parameters. In our case, only 4 basic shapes of triangles need to be considered, Figure 6., which is denoted by s.

Summing up the contributions of the three triangles, we can obtain the viscoelastic forces applied to the nodal points as:

$$F_{visela} = \begin{bmatrix} f_i \\ f_j \\ f_k \\ f_{cent} \end{bmatrix} = \begin{bmatrix} f^1_i & & +f^3_i \\ f^1_j & +f^2_j & \\ & +f^2_k & +f^3_k \\ f^1_{cent} & +f^2_{cent} & +f^3_{cent} \end{bmatrix}, \quad (10)$$

where $f^m_p = K_{\Delta m}u_p + B_{\Delta m}\dot{u}_p$ (m =1, 2, 3and p =i, j, k, *cent*) describe the contribution of triangle m to the viscoelastic forces and f_i through f_{cent} denote the total viscoelastic forces applied to nodal points P_i P_j P_k and P_{cent}. In the example of triangle $\Delta_{P_iP_jP_c}$, illustrated in Figure 6 (a) we have

$$\begin{bmatrix} f^1_i \\ f^1_j \\ f^1_{cent} \end{bmatrix} = K_{\Delta 1}\begin{bmatrix} u^*_i \\ u^*_j \\ u^*_{cent} \end{bmatrix} + B_{\Delta 1}\begin{bmatrix} \dot{u}^*_i \\ \dot{u}^*_j \\ \dot{u}^*_{cent} \end{bmatrix}.$$

Note that the centroid node P_{cent} is defined as the third node in every triangle. Let $f^m_{m,1}$, $f^m_{m,2}$ and f^m_{cent} be the contribution of forces in triangle m. In the LCR, the apexes P_i P_j P_k are supposed to be transient fixed, so we have $u^*_{p'} = \dot{u}^*_{p'} = 0$ (p'=i, j, k), that yields

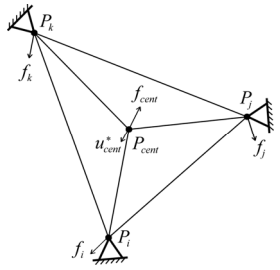

Figure 5. Local Constraint Region '$P_iP_jP_k$ - P_{cent}'

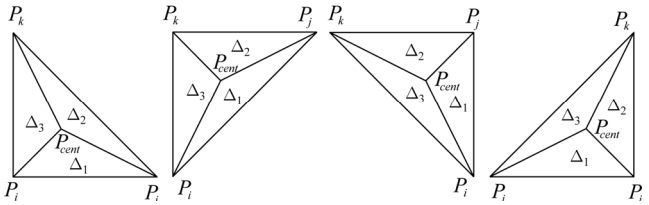

Figure 6. Basic shapes of triangles in tissue's frame

$$\begin{bmatrix} f^m_{m,1} \\ f^m_{m,2} \\ f^m_c \end{bmatrix} = K_{\Delta m}\begin{bmatrix} 0 \\ 0 \\ u^*_{cent} \end{bmatrix} + B_{\Delta m}\begin{bmatrix} 0 \\ 0 \\ \dot{u}^*_{cent} \end{bmatrix} = \begin{bmatrix} K^{13}_{\Delta m} \\ K^{23}_{\Delta m} \\ K^{33}_{\Delta m} \end{bmatrix}u^*_{cent} + \begin{bmatrix} B^{13}_{\Delta m} \\ B^{23}_{\Delta m} \\ B^{33}_{\Delta m} \end{bmatrix}\dot{u}^*_{cent}.$$

A set of viscoelastic forces at nodal points of the local region can be derived as follows:

$$F_{visela} = \begin{bmatrix} f_i & f_j & f_k & f_{cent} \end{bmatrix}^T = \begin{bmatrix} K_{L1} \\ K_{L2} \end{bmatrix}u^*_{cent} + \begin{bmatrix} B_{L1} \\ B_{L2} \end{bmatrix}\dot{u}^*_{cent}. \quad (11)$$

where

$$K_{L1} = \begin{bmatrix} K^{13}_{\Delta 1} + K^{13}_{\Delta 3} \\ K^{23}_{\Delta 1} + K^{13}_{\Delta 2} \\ K^{23}_{\Delta 2} + K^{23}_{\Delta 3} \end{bmatrix}, \quad B_{L1} = \begin{bmatrix} B^{13}_{\Delta 1} + B^{13}_{\Delta 3} \\ B^{23}_{\Delta 1} + B^{13}_{\Delta 2} \\ B^{23}_{\Delta 2} + B^{23}_{\Delta 3} \end{bmatrix},$$
$$K_{L2} = \sum_{m=1}^{3} K^{33}_{\Delta m}, \quad B_{L2} = \sum_{m=1}^{3} B^{33}_{\Delta m}.$$

In step II, all these matrices K, B are calculated before the simulation. And we have the forces at nodal points in local element for further use as follows:

$$F_{i,j,k} = K_{L1}u^*_{cent} + B_{L1}\dot{u}^*_{cent}$$
$$f_{cent} = K_{L2}u^*_{cent} + B_{L2}\dot{u}^*_{cent} . \quad (12)$$

3) Step III: $f_{cent} \rightarrow f_{tip}$

To map the force back on the tip node, according to the virtual work principle $f^T_{cent}u^*_{cent} = f^T_{tip}u^*_{tip}$, we have

$$\underbrace{\left(K_{L2}\overbrace{u^*_{cent}}^{StepI} + B_{L2}\overbrace{\dot{u}^*_{cent}}^{StepI}\right)}_{StepII} u^*_{cent} = f^T_{tip}u^*_{tip} . \quad (13)$$

Combining (8) and (9) with (13), the tip force f_{tip} is obtained.

As a result, the output of the local system mainly comprises two output components: one is the force vector $F_{i,j,k}$ of the three triangle apexes, which is applied on the whole tissue body as external force constraints influenced by the needle tip; the other is the tip force f_{tip}, which is regarded as a factor for rupture condition as well as the reaction force at the needle tip.

C. Surface Contact and Rupture

In the simulation of surface contact, we need to decide when we should add the contact-constraint to the equation of motion. We define the area of a triangle as

$$S_{\Delta P_i P_j P_k} = \frac{1}{2}\begin{pmatrix}\xi_i & \xi_j & \xi_k\end{pmatrix}\begin{pmatrix}\eta_j - \eta_k \\ \eta_k - \eta_i \\ \eta_i - \eta_j\end{pmatrix} \quad (14)$$

Note that the sign of the area is positive if the nodes of the triangle follow a clockwise order; otherwise the sign will be negative. We suppose that any needle node P within one of the triangles on the tissue body indicates that the two objects are in contact. Note that when a node is inside a triangle, the signs of all areas of the triangle separated by these four nodes are positive. So we define the contact condition as:

$$Min\left\{S_{\Delta PP_jP_k}, S_{\Delta P_iPP_k}, S_{\Delta P_iP_jP}\right\} \geq 0 \quad (15)$$

After contact with the surface, the deformation and forces between the needle and tissue can be calculated automatically by solving the dynamic equation of motion with the constraints added at the contact nodes. Force at the needle tip increases before puncturing the tissue as the needle is moving. The puncture event happens when the rupture force threshold is exceeded. For the simplest case of our simulation, the tip force is calculated using LCM as described above. Defining the threshold of rupture force as f_r, the rupture condition is considered as:

$$f_{tip} \geq f_r , \quad (15)$$

where f_r mainly depends on the material features of the tissue, the area of tissue in contact with the needle tip and the velocity of insertion according to the fracture mechanism [10]. At the moment considered to be a rupture event, the node on the needle tip will lose its constraints as it is supposed to be in contact with the 'Crack'.

IV. Simulation Results

In this section, we simulate a simple insertion process using LCM considering contact and rupture events. As mentioned in section III, in the simulation the tissue is proposed to be a rectangle of 80 × 80mm^2 with viscoelastic behavior. Elastic and viscous moduli are E=20kPa and c=20kPa. Poisson ratios are given by $\upsilon = \upsilon^{vis}$=0.35. Deformation and force information are calculated as the simulation results.

A. Deformation of Tissue

The insertion procedure in this simulation includes surface contact, tissue rupture and release. A rigid needle is inserted downward into the tissue body during the first 2s at a velocity of 0.3mm/s, and then held static for 2s. Deformed tissue shapes at some time points shown in Figure 7. When t=0.667s the needle's tip first reaches the top of tissue, contacts with tissue and the tissue deforms, (a); as the needle moves down, both the deformation of tissue and the force at needle-tip increase (b-c); when the needle-tip force is up to the breakpoint, we suppose a "Rupture" happens, (d). Needle stops at t=2s and last for 2 seconds; tissue releases, (e-f).

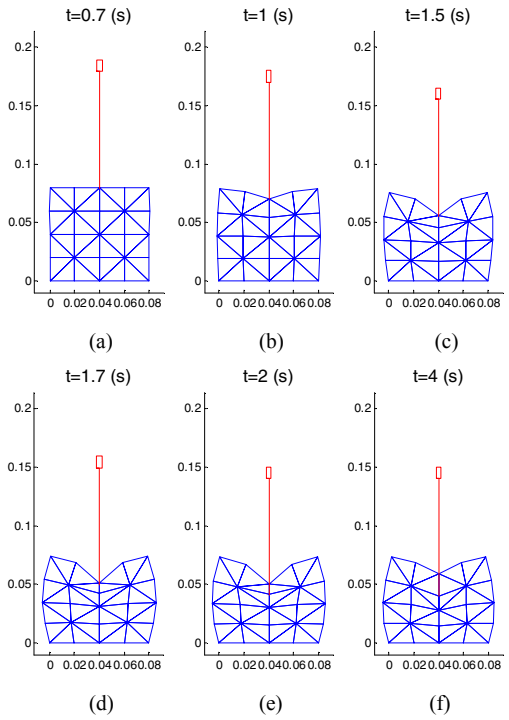

Figure 7. Example of a rigid needle penetrating viscoelastic tissue in 2D. (a) Needle contacts tissue surface. (b) Unbroken suface deforms. (c) Rupture occurs. (d) Needle penetrates tissue. (e)-(f) Needle stops, tissue released.

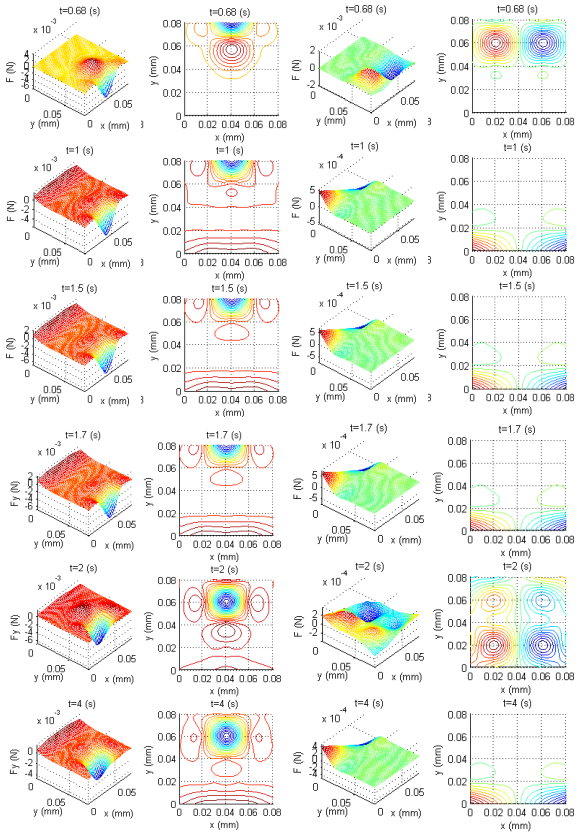

(a) (b) (c) (d)

Figure 8. Distribution of force on tissue (a-b) y-axis and (c-d) x-axis

B. Force Distributions

Correspondingly at these time points, force distributions of tissue are shown in Figure 8, in both x-axis (a-b) and y-axis (c-d) respectively. It shows that when needle contact with tissue stress distribution is concentrated near the needle tip, as the needle moves down, forces at the tip increase until a rupture event occurs. When the needle stops, the stress inside the tissue spreads and the tissue becomes to release. Note that, we didn't include friction force in this simulation, so the force distribution only shows the influences from the needle tip.

V. CONCLUSIONS AND FUTURE WORK

In this paper, we presented a Local Constraint Method for dynamic modeling and simulation of needle insertion based on FEM to avoid the need to continuously update the mesh which is usually required during needle insertion events especially the event of rupture. In our method we considered needle influence on tissue inside a local region as a sub-system to calculate the forces at related nodal points; and we applied the forces as constraints back to the whole tissue body. A simple case of needle insertion simulation, which considered contact and rupture, verified the applicability of this method. The simulation shows that LCM can be employed to simulate a dynamic model for needle interaction with deformable tissue properties; and represent the deformation and interaction force information for both needle and tissues. In the future, we plan to verify the interaction simulation results by experiments including both deformation and force information. Modeling for rupture, with consideration to needle shape and movement, and the influence of friction will also be investigated.

REFERENCES

[1] Abolhassani, N., R. Patel. Needle insertion into soft tissue: a survey. Medical Engineering & Physics 29(4), 2007, pp. 413-431.

[2] DiMaio, S. P. and S. E. Salcudean. Needle insertion modeling and simulation. Robotics and Automation, IEEE Transactions on 19(5), 2003, pp. 864-875.

[3] DiMaio, S. P. and S. E. Salcudean. Interactive simulation of needle insertion models. Biomedical Engineering, IEEE Transactions on 52(7) , 2005, pp. 1167-1179.

[4] Alterovitz, R., K. Goldberg, *et al*., Needle insertion and radioactive seed implantation in human tissues: simulation and sensitivity analysis. Robotics and Automation, 2003.

[5] Nienhuys, H. W. and A. F. van der Stappen, A computational technique for interactive needle insertions in 3D nonlinear material. Robotics and Automation, 2004. Proceedings. ICRA '04. 2004 IEEE International Conference on.

[6] Okamura, A. M., C. Simone, *et al*., Force modeling for needle insertion into soft tissue. Biomedical Engineering, IEEE Transactions on 51(10) , 2004, pp. 1707-1716.

[7] Kataoka, H., T. Washio, *et al*., Measurement of the tip and friction force acting on a needle during penetration. Proceedings of the 5th International Conference on Medical Image Computing and Computer-Assisted Intervention-Part I, Springer-Verlag, 2002, pp. 216-223.

[8] Webster, R. J., J. S. Kim, *et al*., Nonholonomic modeling of needle steering. The International Journal of Robotics Research 25(5-6), 2006, pp. 509-525.

[9] Misra, S., K. B. Reed, *et al.*, Mechanics of flexible needles robotically steered through soft tissue. The International Journal of Robotics Research 29(13), 2010, pp. 1640-1660.

[10] Mahvash, M. and P. E. Dupont, Mechanics of dynamic needle insertion into a biological material. Biomedical Engineering, IEEE Transactions on 57(4), 2010, pp. 934-943.

[11] Misra, S., Ramesh K. T., Okamura A. M., Modeling of tool-tissue interactions for computer-based surgical simulation: a literature review, Presence (Camb), 2008 October 1, 17(5), pp. 463

[12] S. T. Lin and J. N. Huang, Stabilization of Baumgarte's using the Runge-Kutta approach, IEEE Conference on Intelligent Robots and Systems, October 1998.